In Vivo High-Frequency, Contrast-Enhanced Ultrasonography of Uveal Melanoma in Mice: Imaging Features and Histopathologic Correlations

Qing Zhang,[1,2,3] *Hua Yang,*[1,3] *Shin J. Kang,*[1] *Yanggan Wang,*[4] *Geoffrey D. Wang,*[5] *Tonya Coulthard,*[6] *and Hans E. Grossniklaus*[1,7]

Purpose. To evaluate the usefulness of in vivo imaging of uveal melanoma in mice using high-frequency contrast-enhanced ultrasound (HF-CE-US) with 2D or 3D modes and to correlate the sonographic findings with histopathologic characteristics.

Methods. Fourteen 12-week-old C57BL6 mice were inoculated into their right eyes with aliquots of 5×10^5/2.5 μL B16LS9 melanoma cells and were randomly assigned to either of two groups. At 7 days after inoculation, tumor-bearing eyes in group 1 ($n = 8$) were imaged using HF-CE-US to determine the 2D tumor size and relative blood volume; eyes in group 2 ($n = 6$) were imaged by 3D microbubble contrast-enhanced ultrasound, and the tumor volume was determined. Histologic tumor burden was quantified in enucleated eyes by image processing software, and microvascular density was determined by counting von Willebrand factor-positive vascular channels. Ultrasound images were evaluated and compared with histopathologic findings.

Results. Using HF-CE-US, melanomas were visualized as relatively hyperechoic regions. The intraobserver variability of sonographic measurements was 9.65% ± 7.89%, and the coefficient of variation for multiple measurements was 7.33% ± 5.71%. The correlation coefficient of sonographic volume or size and histologic area was 0.71 ($P = 0.11$) and 0.79 ($P = 0.32$). The relative blood volume within the tumor demonstrated sonographically correlated significantly with histologic tumor vascularity ($r = 0.83$; $P < 0.001$).

Conclusions. There was a positive linear correlation between sonographic tumor measurements and histologic tumor burden in the mouse ocular melanoma model. Contrast-enhanced intensity corresponded with microvascular density and blood volume. HF-CE-US is a real-time, noninvasive, reliable method for in vivo evaluation of experimental intraocular melanoma tumor area and relative blood volume. (*Invest Ophthalmol Vis Sci.* 2011;52:2662–2668) DOI:10.1167/iovs.10-6794

Malignant melanoma of the uvea is the most common primary intraocular malignancy in adults; it occurs in approximately six of every 1 million persons.[1–4] Tumor size is one of the most important factors in determining both treatment and prognosis for uveal melanoma.[5–7] Apical tumor height and largest tumor diameter are risk factors for extrascleral extension, posttreatment recurrence, and metastasis.[7–9] Accurate measurements of tumor apical height and basal diameter are critical for monitoring tumor growth and establishing treatment, such as in choosing brachytherapy plaque size and radiation dose.[10,11]

Ultrasound has been extensively used as an effective diagnostic tool in the evaluation of uveal melanoma since the 1950s, when A-mode ultrasound was first applied. In general, most uveal melanomas are dome or mushroom shaped, and each dome or mushroom exhibits a unique growth progression. They may appear biconvex, spheroid, ellipsoid, or hemiellipsoid during their growth[12–14] and eventually become irregular as they break through the Bruch's membrane. Although apical height and basal diameter measurements are used for monitoring tumor growth or regression, 3D volume, which is independent of tumor shape, offers an objective estimate of tumor size and may be important in the evaluation of melanoma progression.[15–17]

Another essential criterion for evaluating uveal melanomas in standardized A-scan is the evidence of blood flow inside the tumor.[18] However, clinical visualization of uveal melanoma microcirculation by A-scan or B-scan is limited. Microbubbles have recently been developed as ultrasound contrast agents to increase the acoustic backscatter of ultrasound, making this technology useful for contrast enhancement of vascular anatomy and blood flow within tumors.[19,20] These gas-filled microbubbles measure 1 to 10 μm in diameter, scatter ultrasound energy, and can be used as red blood cell tracers in densely vascularized tissues. Various ultrasound contrast agents (including Albunex [Mallinckrodt Inc., Hazelwood, MO], Definity [Lantheus Medical Imaging, Billerica, MA], Imagent [IMCOR Pharmaceuticals, Inc., San Diego, CA], Sonovue [Bracco Diagnostics, Princeton, NJ], and Levovist [Schering AG, Berlin, Germany]) have been developed and are extensively used in cardiology and radiology.[21–24]

In this study, we evaluated the usefulness of high-frequency microbubble contrast-enhanced 2D and 3D ultrasound in vivo imaging of a mouse ocular melanoma model. We then correlated the ultrasound images with histologic findings.

From the Departments of [1]Ophthalmology, [4]Pediatrics and Children's Healthcare of Atlanta and [7]Pathology, Emory University School of Medicine, Atlanta, Georgia; the [2]Department of Ophthalmology, Central South University Second Xiangya Hospital, Hunan, China; the [5]Department of Pharmaceutical and Biomedical Sciences, University of Georgia, Athens, Georgia; and [6]VisualSonics, Toronto, Ontario, Canada.

[3]These authors contributed equally to the work presented here and should therefore be regarded as equivalent authors.

Supported in part by National Institutes of Health Grants R01 CA126557 (HEG) and R24 EY017045 (HEG) and by an unrestricted departmental grant from Research to Prevent Blindness, Inc..

Submitted for publication October 27, 2010; revised December 7, 2010; accepted December 8, 2010.

Disclosure: **Q. Zhang**, None; **H. Yang**, None; **S.J. Kang**, None; **Y. Wang**, None; **G.D. Wang**, None; **T. Coulthard**, None; **H.E. Grossniklaus**, None

Corresponding author: Hans E. Grossniklaus, Department of Ophthalmology, Emory University School of Medicine, L.F. Montgomery Ophthalmic Pathology Laboratory, BT428 Emory Eye Center, 1365-B Clifton Road, Atlanta, GA 30322; ophtheg@emory.edu.

Materials and Methods

Cell Cultures

Mouse melanoma cell line B16LS9 (courtesy of Dario Rusciano, Friedrich Miescher Institute, Basel, Switzerland) was cultured at 37°C in 5% CO_2 in complete culture medium (RPMI-1640 with HEPES and L-glutamine, 10% fetal bovine serum, 1% nonessential amino acids, 1% sodium pyruvate solution, 1% MEM vitamin solution, 1% antibiotic-antimycotic solution containing 100 U/mL penicillin G, 250 ng/mL amphotericin B, and 100 μg/mL streptomycin solution [Gibco, Grand Island, NY]).

Animals

Fourteen 12-week-old female C57BL/6 mice (Charles River, Wilmington, MA) housed under conventional conditions in plastic cages in the Department of Animal Resources were used for this investigation. All procedures were conducted in accordance with the ARVO Statement for the Use of Animals in Ophthalmic and Vision Research and were approved by the Emory University Institutional Animal Care and Use Committee.

Growth of Choroidal Melanoma Xenografts

Aliquots of 5×10^5/2.5 μL B16LS9 cells were inoculated into the suprachoroidal space of the right murine eye using a transscleral technique that allows the inoculated cells to remain in the eye. The mice were anesthetized with a ketamine/xylazine mixture (administered intraperitoneally). A tunnel was prepared from the superior limbus within the sclera to the suprachoroidal space with a 30-gauge needle under a dissection microscope. A 2.5-μL suspension of cells was inoculated into the suprachoroidal space through the needle track with a 10-μL glass Hamilton syringe (Hamilton, Reno, NV) equipped with a ¾-inch-long beveled 32-gauge needle. No tumor cell reflux occurred, and the subconjunctival space remained free of tumor cells. The mice were randomly assigned into two groups.

High-Frequency, Contrast-Enhanced Ultrasound Imaging of Mouse Eyes

On day 7 after the intraocular inoculation of tumors, in vivo high-frequency, contrast-enhanced ultrasound (HF-CE-US) imaging was performed with a dedicated small-animal, high-resolution imaging system (VisualSonics, Inc., Toronto, ON, Canada) with a 40-MHz transducer. Mice in group 1 ($n = 8$) were imaged with Vevo 770 2D contrast mode, and mice in group 2 ($n = 6$) were imaged with Vevo 2100 3D contrast mode. Before the imaging session, mice were anesthetized as described previously and were placed on a flat heating pad. The heart rate was monitored and remained at approximately 400 beats per minute. Sterile ultrasound gel (Aquasonic 100; Parker Laboratories, Fairfield, NJ) was placed on the right eye bearing the uveal melanoma xenograft. The probe (RMV 707B; VisualSonics, Inc.) was positioned so that the cornea was to the superior of B-scan imaging, and the probe was then adjusted until the tumor was visible centrally on the screen of the ultrasound unit within the focal zone. Thereafter, the probe was fixed mechanically to improve the accuracy of intensity comparison and subtraction in a given slice. As suggested by the manufacturer, the parameters of the ultrasound system were initially optimized as described here for standard values for imaging small animal tissues: 50% transmitted power, 52-dB dynamic range, and 6.00 × 6.00-mm field of view. Baseline images without contrast agent were recorded. For contrast-enhanced imaging, a vial of contrast agent (MicroMarker; VisualSonics) was reconstituted with sterile saline and gently agitated. A 50-μL bolus containing a final count of 1.0×10^8 microbubbles, which had been optimized for tumor imaging, was injected through the mice tail vein with a fixed needle (Butterfly 625; Abbott, Dublin, Ireland), and a real-time cine loop of contrast-mode imaging was immediately recorded. The 3D volumetric data were obtained according to the image acquisition protocol with 3D image reconstruction and visualization software. When the 3D images were being processed, the ultrasound scan head linearly translated across the mouse's eye on the 3D motor system, and 2D images were acquired at regular spatial intervals so that they were parallel and uniformly spaced at 30-μm intervals over the entire image. Thereafter, 3D images were constructed and displayed through the parallel 2D image planes. At the end of all studies, the tumor-bearing right eyes were oriented, marked, enucleated, and submitted for routine histology processing.

Imaging Data Processing and Analysis

The series of digital scans was converted into AVI videos. Contrast-enhanced images were processed on the basis of subtraction from all points in the time course to eliminate the noncontrast baseline signal. The region of interest (ROI) in each image was traced manually around the entire tumor area, and the final size was computed using the manufacturers' software measurement tools. Three-dimensional volumetric measurements were obtained by segmentation of 10 to 12 parallel planes through the 3D images. The tumor was manually outlined on the initial plane at the lower pole; the segmentation plane was then moved until the tumor was completely segmented. The volume was automatically computed using the trapezoidal rule, where the volume between two slices was calculated as the average of the two outlined areas multiplied by the interslice distance. Consequently, the interslice volumes were summed to obtain the total 3D volume. Plots of the contrast region time-intensity curves were normalized by subtracting the mean precontrast (baseline) intensity value from each intensity level. From the pulse destruction curves, the contrast replenishment portion of the curve was fit with a two-parameter exponential recovery curve: $CI(t) = A(1 - e^{-Bt})$, where CI represents video intensity, A represents the microvessel cross-sectional area indicating relative blood volume, and B represents the slope of the exponential portion of the curve standing for the microbubble velocity.

Estimation of Tumor Area from Histologic Sections

All enucleated mouse eyes were fixed in 10% formalin, dehydrated in increasing concentrations of alcohol, and cleared in xylene. Careful attention was paid to the labeling of each specimen to ensure that it was embedded in paraffin in the same transaxial plane as the specimen imaged by ultrasound. Serial 8-μm sections were prepared, and every third slide was stained with hematoxylin-eosin. Ten sections with the largest tumor area in each eye were photographed at ×40 magnification (DP 10; Olympus, Tokyo, Japan). The tumor size was determined with ImageJ software (developed by Wayne Rasband, National Institutes of Health, Bethesda, MD; available at http://rsb.info.nih.gov/ij/index.html).

Immunohistochemistry

One slide containing five sections from each mouse eye was immunostained for von Willebrand factor (vWF) using a standard blood vessel staining kit (Millipore, Billerica, MA). The slides were microwaved in citrate buffer, pH 6.0, at 95°C for 10 minutes for antigen retrieval. Endogenous peroxidase activity was eliminated by the application of hydrogen peroxide. The sections were then incubated with the primary antibody overnight at 4°C in a humidity chamber. The biotinylated antibody to the secondary antibody was then applied, and amino ethyl-carbazole (AEC) was used as a chromogen. Known positive controls were immunostained, and negative controls were prepared by not applying the primary antibody. The slides were counterstained with hematoxylin, coverslipped, and evaluated by light microscopy. Vascular channels were recognized in the tumor using ×100 magnification by identifying the vascular endothelium positive for vWF staining. The portion of tumor with highest vascular density ("hot spots") was examined using ×200 magnification, and the number of blood vessels in the field was counted. The average of three counts of each case was calculated to determine mean microvascular density (MVD).[25]

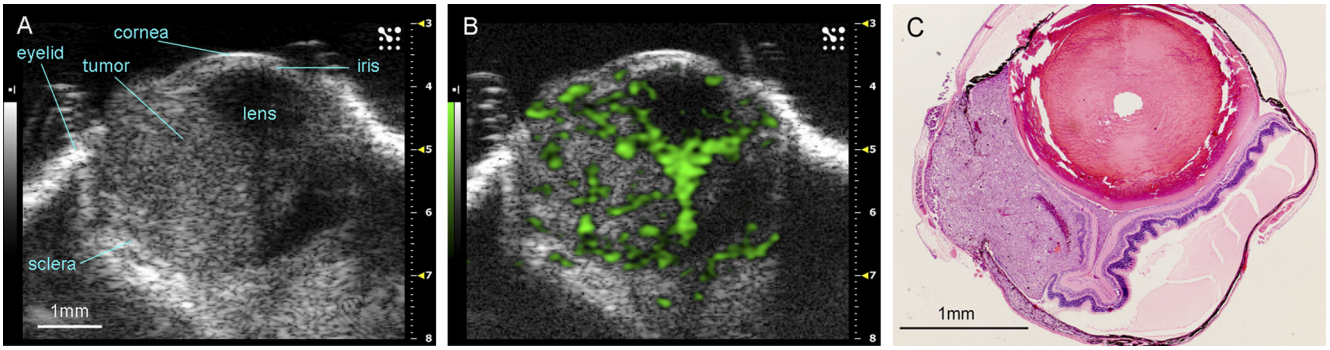

FIGURE 1. Representative example of a uveal melanoma imaged in high-frequency ultrasound before (**A**) and after (**B**) injection of 50 μL contrast agent. Enhancement is present in the tumor and the funnel-shaped detached retina. A pathology specimen obtained from the same case is shown in (**C**) (hematoxylin and eosin, ×40). Disruption of the posterior sclera is an artifact of histology processing.

Statistical Analysis

Results were expressed as the mean ± SD. Two-tailed Student's *t*-tests were used to compare data between histologic sections and HF-CE-US images. Pearson correlation and standard linear regression analysis between variables was examined. In all analyses, $P < 0.05$ was considered statistically significant.

RESULTS

High-Frequency Contrast-Enhanced Ultrasound Imaging of Uveal Melanoma Xenografts

An example of ultrasound imaging of a uveal melanoma before and after contrast administration is shown in Figure 1. The details of ocular structures, including orbit, eyelid, cornea, and the thin layer of iris, could be imaged (Fig. 1A). The lens appeared as a low-echoic oval region, sometimes with a hyperintense arc, in the center of each eye. The tumor appeared as a relatively hyperechoic and heterogeneous region internal to the sclera, showing evidence of some structural detail. With the injection of microbubbles, the contrast-enhanced regions were illustrated with pseudocoloring in green (Fig. 1B). In some cases, a low-echoic retina was observed and highlighted with contrast agents. The hyperechoic, enhanced area could be identified histologically as tumor (Fig. 1C). As the scan head was moved temporally across the right eye, the hyperechoic tumor region changed in size (Fig. 2). Three series of images that displayed the largest area of tumor were obtained, and the average value was taken. This permitted us to obtain comparable ultrasound and histology data of the largest tumor size. In the 3D mode, tumors were imaged and could be displayed as cube or surface views. These data could be rotated, sliced, and analyzed, and the tumor volumes were then calculated by the manufacturer's software. This method is illustrated in Figure 3, which shows a manually drawn outline of the tumor in a sample cross-sectional 2D image "sliced" from a 3D ultrasound image.

Tumor Size/Volume Measurements

At day 7, all tumors were visualized by the B-scans, though there was variability such as those shown in Figure 4. The average size of tumor in group 1 with 2D mode imaging was 1.08 ± 0.08 mm^2 ($n = 8$); the average tumor volumes of group 2 mice with 3D mode imaging was 1.90 ± 0.67 mm^3 ($n = 6$). Using histologic measurements, the average tumor area was 0.86 ± 0.56 mm^2 and 1.41 ± 0.65 mm^2 in groups 1 and 2, respectively. Significant correlations were found between the histologic measurements and sonographic 2D tumor sizes (Fig. 5A; $r = 0.71$; $P > 0.05$) and 3D mode tumor volume (Fig. 5B; $r = 0.79$; $P = 0.32$). The interseries coefficient of variation (relative SD) was independent of the tumor size, and its mean value was $7.33\% \pm 5.71\%$. To evaluate the intraobserver variability, image series were analyzed by the same observer on two different days in a blinded fashion; the mean intraobserver coefficient of variation was $9.65\% \pm 7.89\%$.

Tumor Vasculature Measurements

The relative blood volume of tumors was calculated as shown in Figures 6A and 6B. In this plateau, the A value of the time intensity curve represented relative blood volume in the tumor area, and the B value represented the relative blood velocity. The average A value and B value was 151.14 ± 40.00 and 0.6 ± 0.19, respectively. With immunostaining for vWF (Fig. 6C), the average microvascular density of uveal melanomas was 14.54 ± 4.04. The correlation coefficient of sonographic relative blood volume and histologic MVD was 0.83 (Fig. 6D; $P < 0.001$). There was no correlation between relative blood velocity and MVD ($r = -0.23$; $P < 0.0001$).

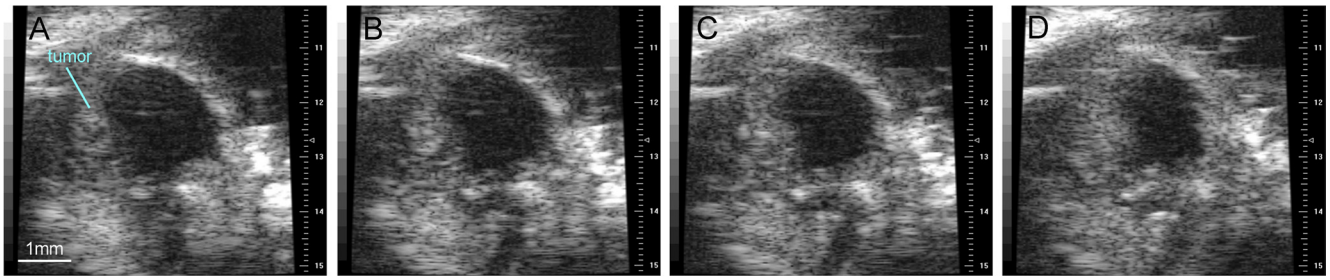

FIGURE 2. Series of images shows the ROI in a tumor-bearing eye was changed in size (**A–D**) as the scan head was moved from the nasal to the temporal side.

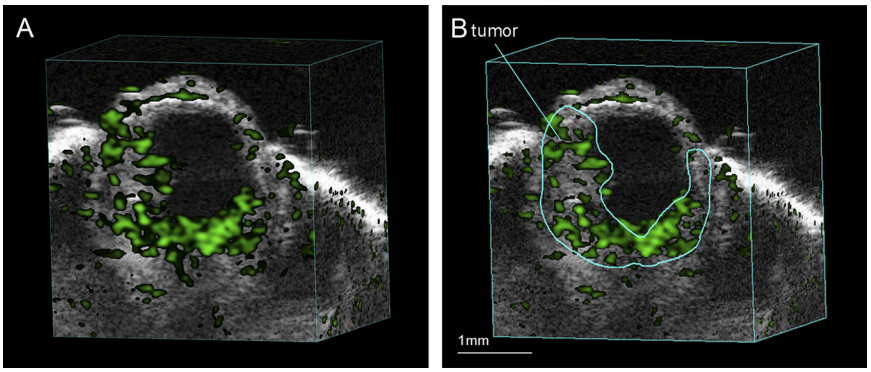

FIGURE 3. Contrast mode image showing a representative 3D cube view (**A**). Note the manually drawn outline of the tumor in a sample cross-sectional 2D image "sliced" from a 3D ultrasound image (**B**).

DISCUSSION

High-Frequency Imaging of Uveal Melanoma Xenografts

Portability, real-time capacity, and rapid imaging speed are advantages of ultrasound over other imaging methods, such as magnetic resonance imaging (MRI).[26] The ultrasound system used in this study allowed for measurements of sequences of images that were saved as cine loops. This permitted multiple series of images to be collected while the mice were under short-duration anesthesia, which could be repeated and sequentially followed. The reproducibility of the measurements estimated by the same observer on the same series of B-scan images was very good. High-frequency ultrasound (40 MHz) permitted the visualization of our mouse ocular melanoma model with high resolution, allowing visualization of the cornea, iris, anterior chamber, ciliary body, and posterior pole. The tumors were relatively hyperechoic compared with most other intraocular structures. Small tumors, such as the one with the largest area in our study, 0.58 mm^2, can be imaged. This technique provided reproducible, reliable, and easily generated quantitative measurements, especially considering the small size of the mouse eye.

3D Volumetric Measurements of Uveal Melanoma Xenografts

Calculation of uveal melanoma tumor volume by mathematical modeling is limited by assumptions made regarding the shape

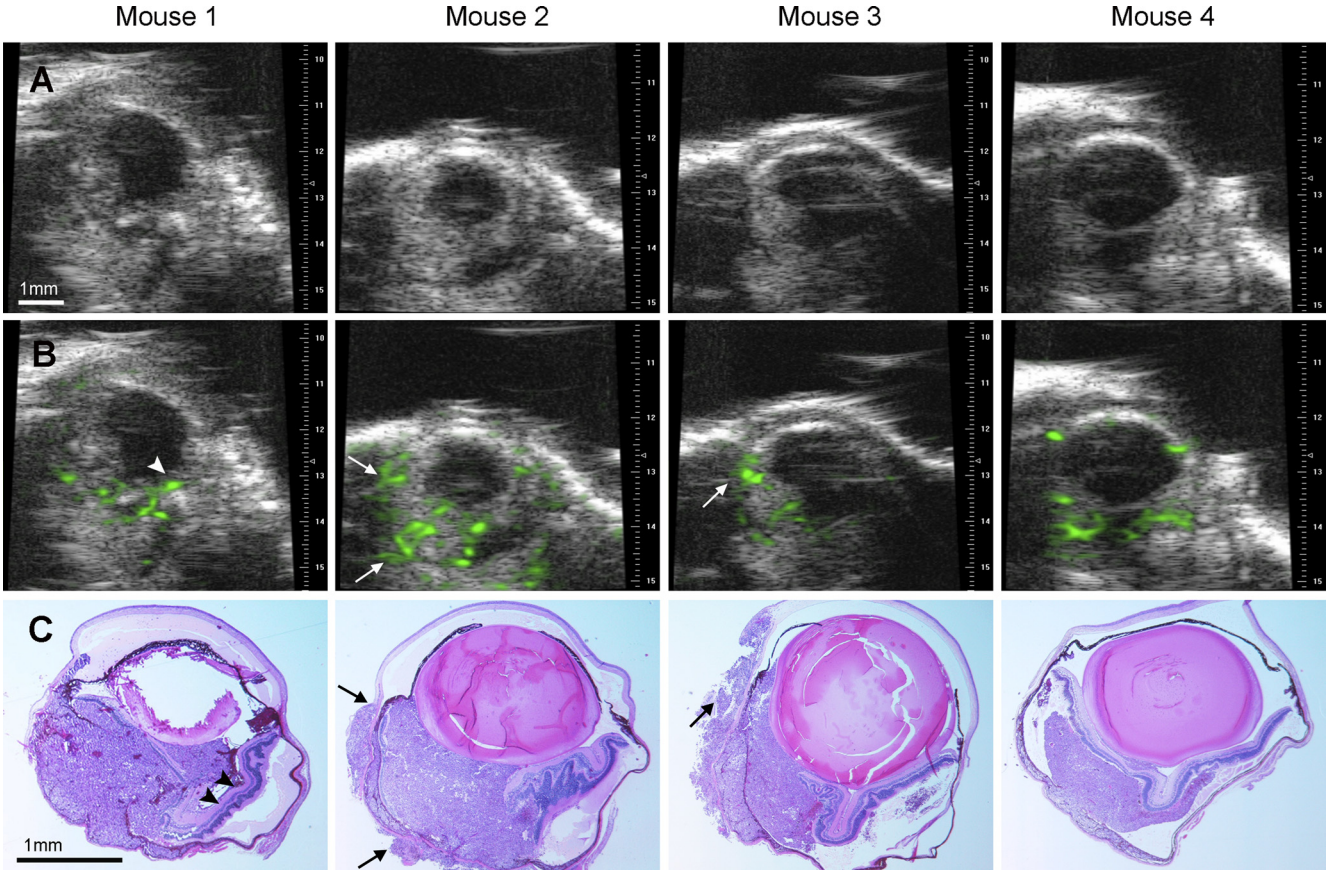

FIGURE 4. Samples of uveal melanomas imaged in four mice with 2D ultrasound before (**A**) and after (**B**) contrast enhancement and correlated histologic sections (**C**, hematoxylin and eosin, ×40). Funnel-shaped retinal detachment in mouse 1 (*arrowheads*) and extraocular extension of tumor in mouse 2 and mouse 3 was observed with enhancement (*arrows*).

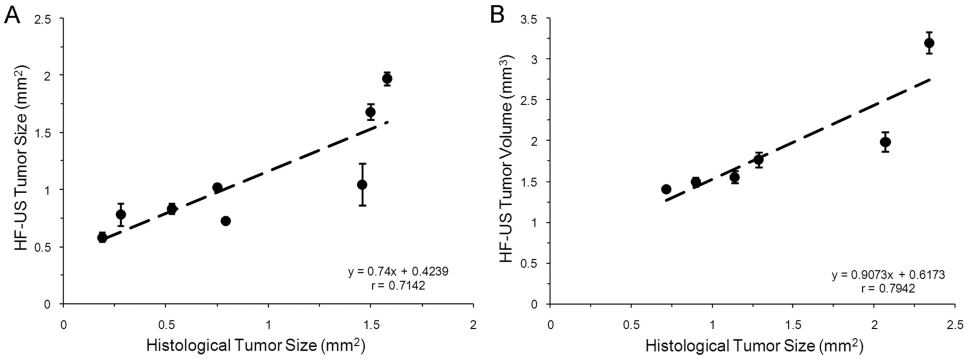

FIGURE 5. Scatterplots show the positive relationship between histologic measurements and sonographic data measured by 2D mode (**A**) and 3D mode (**B**).

of the tumor.[15–17] Singh et al.[27] evaluated five published methods of estimating uveal melanoma volumes and concluded that these methods are inconsistent; hence, caution is needed when volume measures are used for prognostic classification. The closest approximations of uveal melanoma tumor volume are likely achieved by 3D ultrasound techniques. Previous studies have reported that the 3D ultrasound method provides images and measurements with better accuracy, precision, and reproducibility than the 2D method.[28–31] In our study, tumor size or volume determined from ultrasound and histologic sections correlated significantly, with 3D images displaying better estimates than 2D images of histologically determined tumor volume. With the 3D mode, the volume image is "sliced" into a series of uniformly spaced, parallel 2D images, which are stored as a cine loop. After imaging, the cross-sectional area of the tumor in each slice is manually outlined as part of the interactive software. The sum of these areas, multiplied by the inter-slice distance, then provides a reconstruction of a 3D block.

Microbubble Contrast-Enhanced Imaging of Uveal Melanoma Xenografts

Blood flow, blood volume, vascular density, and vascular permeability are anatomic parameters associated with tumor vascularity.[32] The freely diffusible nature of contrast agents limits the assessment of tumor vasculature with MRI, whereas positron emission tomography has spatial resolution limitations. Previous studies have shown correlations between histologic microvascular density and blood flow identified with lower cost and portable color power Doppler sonography of human breast and prostate carcinoma.[33,34] However, the flow sensitivity of power Doppler imaging is limited to vessels larger than 100 μm, which is a major disadvantage because much tumor perfusion occurs at the capillary level.

The introduction of small-microbubble contrast agents in high-frequency sonography has allowed the depiction of tumor vessels smaller than 50 μm in diameter. When used as ultrasound contrast agents, microbubbles have a true blood pool distribution, which gives ultrasound the capability to quantify local blood flow and fractional blood volume.[19,20] Toxicologic and pharmaceutical studies in animals and clinical trials have confirmed the safety and efficacy of microbubble-contrast-enhanced ultrasound.[35–37] Microbubbles have been used extensively in clinical practice in cardiology and radiology. Although the combination of microbubbles and ultrasound is relatively new in ophthalmology, there is clinical potential for this combination. With a low-pressure, high-frequency, nondestructive acoustic pulse, the microbubble expands and contracts with

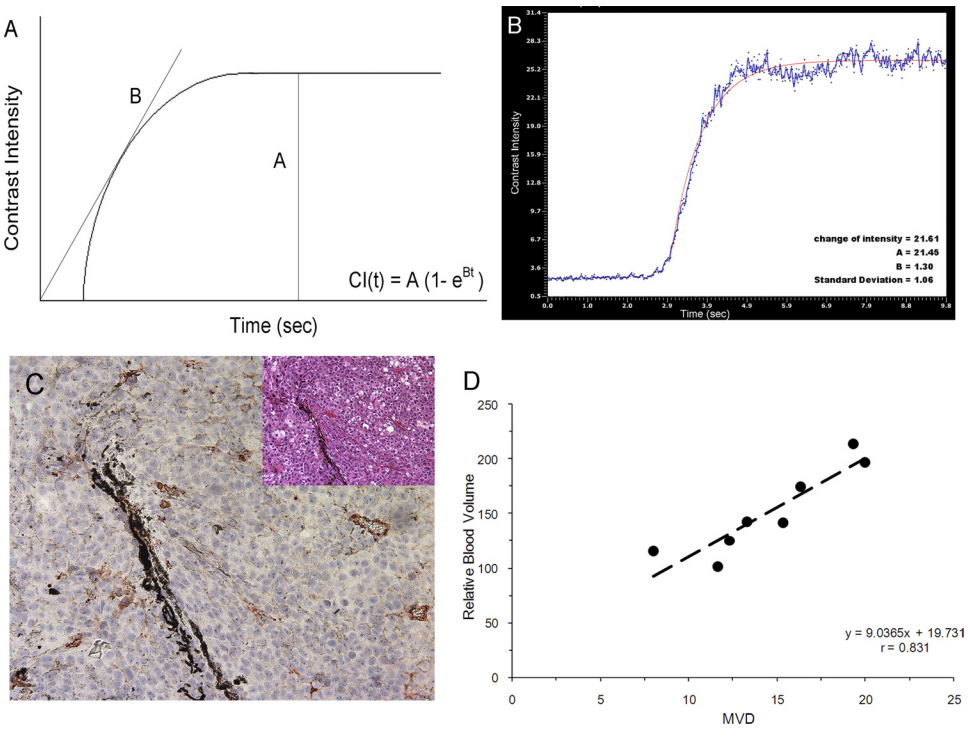

FIGURE 6. (**A**) Schematic depiction of the method used to assess tissue perfusion with contrast ultrasound. On the *y*-axis is peak intensity as a measure of microbubble contrast retention in an ROI. On the *x*-axis is the replenishment time. *Straight lines*: nonlinear square fitting of the video intensities with time, which can be depicted with the exponential equation $CI(t) = A(1 - e^{-Bt})$. In this equation, the A value is calculated as the difference in peak intensity between the baseline and steady state, and the B value is derived from the slope of an exponential curve. (**B**) Example of a smoothed time-intensity curve shows enhancement in the ROI. (**C**) Representative immunohistochemical analysis of endothelial cell density, assessed with an anti-vWF antibody at ×200 magnification (*inset*, hematoxylin and eosin, original magnification, ×200). (**D**) Scatter plots show the positive relationship between relative blood volume and MVD measured by vWF staining.

the applied pressure rarefaction and compression. With this method, the ultrasound signal can be enhanced on echographic scans, flow phenomena can be better seen, and quantitative analysis of organic functions may be provided.

Recent studies have shown strong correlations between MVD and relative tissue blood volume in contrast-enhanced ultrasound of xenographic Lewis lung carcinoma and human gastric cancers[38,39] that are consistent with the data in our murine intraocular melanoma model. MVD is known as a key factor in predicting the survival of patients with uveal melanoma. Although ocular local therapies have been improved to control the growth of the tumor and to try to preserve vision, the mortality rate has remained unchanged. Approximately 50% of patients with uveal melanoma die of hepatic metastasis. MVD most closely parallels the progression of uveal melanoma from primary tumor to metastasis[40]; it is determined by the histology of the nucleated eye. Given that enucleation carries the same survival prognosis as do conservation treatment modalities, local management that preserves vision has become the first choice of treatment rather than enucleation. We show here that sonographic relative blood volume is positively correlated with MVD for the end point experiment, implying that sonographic relative blood volume may provide a new prognostic indicator.

Relatively few reports describe contrast-enhanced ultrasound evaluations of uveal melanomas, and they deal primarily with qualitative image assessments and diagnostic accuracy only.[13–15,18] We have studied 2D and 3D contrast-enhanced, high-frequency ultrasonography for imaging and measurement of a mouse ocular uveal melanoma model. Our data showed that the tumor could be safely imaged with microbubble contrast agent and imaged at high resolution and that the 3D tumor volume could be determined. This technique is promising for its ability to provide noninvasive, reliable, and functional real-time visualization with good resolution.

Our study had several limitations. The number of animals studied was relatively low, which limited the statistical power of the study. The ultrasound system allowed serial timing measurements in the same animal, which meant tumor growth could be followed serially in an animal—an important future application of this technique. The results of this study and the ability to image contrast in small vessels were dependent on the use of high-frequency ultrasound. This worked very well for tumors in the relatively small mouse eye but may not be applicable to choroidal melanoma imaging in the human eye because of the penetration limits at the frequency used. It may be possible to image iris tumors and smaller ciliary body tumors. An improved probe with higher frequency is needed to offer better penetration of the posterior globe with choroidal melanoma. The accuracy of ultrasound techniques for volume determination was dependent on the speed of the 3D imaging and ocular movement. Additionally, it was difficult to extrapolate the use of a fixed probe on an anesthetized animal to the imaging of a moving eye in clinical practice. Most problems that were encountered in 3D imaging and volume determination using lower frequency ultrasound in choroidal melanoma were related to the distortion of the data caused by ocular movement before full image series were obtained.

References

1. Margo CE, Mulla Z, Billiris K. Incidence of surgically treated uveal melanoma by race and ethnicity. *Ophthalmology.* 1998;105:1087–1090.
2. Egan KM, Seddon JM, Glynn RJ, Gragoudas ES, Albert DM. Epidemiologic aspects of uveal melanoma. *Surv Ophthalmol.* 1988;32:239–251.
3. Mahoney MC, Burnett WS, Majerovics A, Tanenbaum H. *Ophthalmology.* 1990;97:1143–1147.
4. Singh AD, Topham A. Incidence of uveal melanoma in the United States: 1973–1997. *Ophthalmology.* 2003;110:956–961.
5. McLean IW, Foster WD, Zimmermann LE. Uveal melanoma: localization, size, cell type and enucleation as risk factors in metastasis. *Hum Pathol.* 1982;13:123–132.
6. Singh AD, Shields CL, Shields JA. Prognostic factors in uveal melanoma. *Melanoma Res.* 2001;11:255–263.
7. Shammas HF, Blodi FC. Prognostic factors in choroidal and ciliary body melanomas. *Arch Ophthalmol.* 1977;95:63–69.
8. Karlsson UL, Augsburger JJ, Shields JA, Markoe AM, Brady LW, Woodleigh R. Recurrence of posterior uveal melanoma after 60Co episcleral plaque therapy. *Ophthalmology.* 1989;96:382–388.
9. Martin JA, Robertson DM. Extrascleral extension of choroidal melanoma diagnosed by ultrasound. *Ophthalmology.* 1983;90:1554–1559.
10. Finger PT. Radiation therapy for choroidal melanoma. *Surv Ophthalmol.* 1997;42:215–232.
11. Packer S, Rotman M. Radiotherapy of choroidal melanoma with ^{125}I. *Ophthalmology.* 1980;87:582–590.
12. Li W, Gragoudas ES, Egan KM. Tumor basal area and metastatic death after proton beam irradiation for choroidal melanoma. *Arch Ophthalmol.* 2003;121:68–72.
13. Richtig E, Langmann G, Mullner K, et al. Calculated tumour volume as a prognostic parameter for survival in choroidal melanomas. *Eye.* 2004;18:619–623.
14. Gass JD. Comparison of uveal melanoma growth rates with mitotic index and mortality. *Arch Ophthalmol.* 1985;103:924–931.
15. Coleman DJ, Silverman RH, RondeauMJ, Lizzi FL,McLean IW, Jakobiec FA. Correlations of acoustic tissue typing of malignant melanoma and histopathologic features as a predictor of death. *Am J Ophthalmol.* 1990;110:380–388.
16. Romero JM, Finger PT, Rosen RB, Iezzi R. Three-dimensional ultrasound for the measurement of choroidal melanomas. *Arch Ophthalmol.* 2001;119:1275–1282.
17. Cusumano A, Coleman DJ, Silverman RH, et al. Three-dimensional ultrasound imaging: clinical applications. *Ophthalmology.* 1998;105:300–306.
18. Collaborative Ocular Melanoma Study Group, Boldt HC, Byrne SF, et al. Baseline echographic characteristics of tumors in eyes of patients enrolled in the Collaborative Ocular Melanoma Study: COMS report no. 29. *Ophthalmology.* 2008;115:1390–1397.
19. Ferrara K, Pollard R, Borden M. Ultrasound microbubble contrast agents: fundamentals and application to gene and drug delivery. *Annu Rev Biomed Eng.* 2007;9:415–447.
20. Marmottant P, Hilgenfeldt S. Controlled vesicle deformation and lysis by single oscillating bubbles. *Nature.* 2003;423:153–156.
21. Kaul S. Microbubbles and ultrasound: a bird's eye view. *Trans Am Clin Climatol Assoc.* 2004;115:137–148.
22. Jakobsen JA. Ultrasound contrast agents: clinical applications. *Eur Radiol.* 2001;11:1329–1337.
23. Yang X. Nano- and microparticle-based imaging of cardiovascular interventions: overview. *Radiology.* 2007;243:340–347.
24. Piscaglia F, Lencioni R, Sagrini E, et al. Characterization of focal liver lesions with contrast-enhanced ultrasound. *Ultrasound Med Biol.* 2010;36:531–550.
25. Grossniklaus HE. Tumor vascularity and hematogenous metastasis in experimental murine intraocular melanoma. *Trans Am Ophthalmol Soc.* 1998;96:721–752.
26. Foster FS, Zhang MY, Zhou YQ, et al. A new ultrasound instrument for in vivo microimaging of mice. *Ultrasound Med Biol.* 2002;28:1165–1172.
27. Singh AD, Terman S, Sculley L. Estimating choroidal melanoma volume: comparison of methods. *Ophthalmology.* 2007;114:1212–1214.
28. Chang FM, Hsu KF, Ko HC, et al. Three-dimensional ultrasound assessment of fetal liver volume in normal pregnancy: a comparison of reproducibility with two-dimensional ultrasound and a search for a volume constant. *Ultrasound Med Biol.* 1997;23:381–389.
29. Gilja OH, Thune N, Matre K, et al. In vitro evaluation of three-dimensional ultrasonography in volume estimation of abdominal organs. *Ultrasound Med Biol.* 1994;20:157–165.

30. Riccabona M, Nelson TR, Pretorius DH, Davidson TE. Distance and volume measurement using three-dimensional ultrasonography. *J Ultrasound Med.* 1995;14:881–886.
31. Tong S, Downey DB, Cardinal HN, Fenster A. A three-dimensional ultrasound prostate imaging system. *Ultrasound Med Biol.* 1996; 22:735–746.
32. Libutti SK, Choyke P, Carrasquillo JA, Bacharach S, Neumann RD. Monitoring responses to antiangiogenic agents using non-invasive imaging tests. *Cancer J Sci Am.* 1999;5:252–256.
33. Nakanouchi T, Okihara K, Kojima M, et al. Possible use of transrectal power Doppler imaging as an indicator of microvascular density of prostate cancer. *Urology.* 2001;58:573–577.
34. Peters-Engl C, Medl M, Mirau M, et al. Color-coded and spectral Doppler flow in breast carcinomas—relationship with the tumor microvasculature. *Breast Cancer Res Treat.* 1998;47:83–89.
35. Main ML, Escobar JF, Hall SA, Grayburn PA. Safety and efficacy of QW7437, a new fluorocarbon-based echocardiographic contrast agent. *J Am Soc Echocardiogr.* 1997;10:798–804.
36. Morel DR, Schwieger I, Hohn L, et al. Human pharmacokinetics and safety evaluation of SonoVue, a new contrast agent for ultrasound imaging. *Invest Radiol.* 2000;35:80–85.
37. Moriyasu F, Itoh K. Efficacy of perflubutane microbubble-enhanced ultrasound in the characterization and detection of focal liver lesions: phase 3 multicenter clinical trial. *AJR Am J Roentgenol.* 2009;193:86–95.
38. Hwang M, Hariri G, Lyshchik A, Hallahan DE, Fleischer AC. Correlation of quantified contrast-enhanced sonography with in vivo tumor response. *J Ultrasound Med.* 2010;29:597–607.
39. Shiyan L, Pintong H, Zongmin W, et al. The relationship between enhanced intensity and microvessel density of gastric carcinoma using double contrast-enhanced ultrasonography. *Ultrasound Med Biol.* 2009;35:1086–1091.
40. Toivonen P, Mäkitie T, Kujala E, Kivelä T. Microcirculation and tumor-infiltrating macrophages in choroidal and ciliary body melanoma and corresponding metastases. *Invest Ophthalmol Vis Sci.* 2004;45:1–6.